Journal of
Ceramic Science
and Technology

J. Ceram. Sci. Tech., 07 [02] 165-172 (2016)
DOI: 10.4416/JCST2015-00080
available online at: http://www.ceramic-science.com

Estimation of Damage in Refractory Materials after Progressive Thermal Shocks with Resonant Frequency Damping Analysis

N. Traon*, T. Tonnesen, R. Telle

GHI/RWTH-Aachen, Aachen, Germany, Institute of Mineral Engineering – Department of Ceramics and Refractory Materials, Aachen, Germany

received December 4, 2015; received in revised form February 1, 2016; accepted February 20, 2016

Abstract

This work correlates damping measurements and the microstructural changes in refractory castables after these have been exposed to thermal shocks in air. In accordance with DIN EN 993 – 11, refractory samples based on tabular alumina with the addition of partially stabilized zirconia (PSZ) were progressively subjected to thermal shocks in air at different temperatures (750, 850, 950 and 1050 °C). White fused alumina samples were also exposed to the same thermal shocks at 950 °C. Evaluation of the thermal shock damage to the high-alumina refractory castables was based on the dynamic Young's modulus and damping characterization data obtained by means of the impulse excitation technique (IET), in accordance with ASTM E1876 – 07. Scanning electron microscopy (SEM) was also performed to enable understanding of the elastic changes in these refractory formulations. The results show that the damping increase in PSZ castables may be explained by crack nucleation and propagation while such phenomena do not occur in WFA castable.

Keywords: Thermal shock, impulse excitation technique, partially stabilized zirconia, Young's modulus, damping

I. Introduction

Service life evaluation and improvement of refractory castables for applications in the metallurgical or the iron and steel industry with regard to physical aspects like thermal shocks and chemical aspects such as corrosive reactions are continuously investigated. The choice of available raw materials for high-performance castables with excellent strength and thermo-mechanical properties plays a central role in refractories and is also directed towards service life optimization. The thermal shock resistance of refractories is currently determined based on assessment of their retained Young's modulus after different thermal shock cycles with the help of the non-destructive impulse excitation technique (IET). However, this standardized method provides only limited information concerning the elastic changes in the refractory castable samples that have been subjected to progressive thermal shocks. A severe depletion of the modulus of elasticity (MOE) is noticeable during crack nucleation followed by a steady decrease of this elastic property corresponding to the crack propagation [1]. In this connection, damping measurements have been established as being more sensitive than those of the modulus of elasticity. Such measurements are extremely useful for homogeneous materials in the determination of phase transformation or microstructural changes like macro- or microscopic crack formation, or thermally activated reorientation of elastic dipoles caused by the movement of oxygen vacancies, etc. [2]. The characterization of such phenomena is more accurate for homogeneous structural ceramics. However, interpretation of the damping changes in brittle materials with heterogeneous microstructure, such as refractory materials, is more challenging. Their microstructure can be seen as anisotropic hard grains and aggregates or crystals consolidated by a mesoscopic bond system containing every kind of defect like cracks, frictional contacts and dislocations at the grain boundaries [3]. This complex material configuration is responsible for non-linear effects that make damping measurements more scattered since the defect density within the material is high. Because of the thermal expansion mismatch between the grog grains and the matrix, cracks nucleate at the level of the grain boundaries and propagate throughout the matrix, consequently increasing the defect density in the castable microstructure and moreover the non-linear response with the number of thermal shock cycles. This non-linear elasticity has already been the subject of studies conducted on rocks with a microstructure similar to that of concrete [4, 5]. The damping property of civil engineering concrete is also a focus of study with regard to the influence of the formulation and particularly the aggregates used on the elastic response of the material [6]. Even so, the study of damping measurement changes combined with SEM analyses can facilitate the understanding and quantification of the role of the defined microstructural changes in the depletion of elastic properties.

Furthermore, to attain a suitable performance during refractory application, aggregates of white fused alumina, tabular alumina, sintered pre-formed spinel, magnesia

* Corresponding author: traon@ghi.rwth-aachen.de

or partially stabilized zirconia or eutectic aggregates are commonly added to calcium-aluminate-cement (CAC)-bonded refractory formulations [7, 8, 9, 10]. The main focus of this study will be on monocrystals of white fused alumina with a theoretically high isotropy compared to that of tabular alumina for instance, and on partially stabilized zirconia added as aggregate to a tabular-alumina-based formulation. Martensitic transformation of this latter raw material accompanied by a non-negligible volume expansion (3 – 5 %) occurs at 1170 °C. Indeed, tetragonal grains of partially stabilized zirconia apply radial stresses in the matrix, so that cracks have to bypass these grains by propagating. In addition to this, the energy of crack propagation can be absorbed by these tetragonal grains transforming into monoclinic ones. The induced volume expansion can lead to the closure of cracks. To limit the effects of grain size distribution on the measurements of the elastic properties measurements, aggregates with a maximum size of 3 mm are used in both formulations.

As documented in Fig. 1, the two studied castable formulations do not demonstrate the same behaviour with regard to the energy of fracture analysed in the wedge splitting test [11]. The formulation based on partially stabilized zirconia (PSZ) withstands high horizontal load with low displacement and the resistance to sample fracture drastically decreases. Such an evolution is typical of materials that present high resistance to crack initiation and low resistance to crack propagation. Thus such castables can withstand high load while cracks propagate throughout the microstructure until the crack density reaches a threshold and the grains of partially stabilized zirconia are no longer able to absorb the energy of the crack propagation. On the other hand, the formulation containing electrofused alumina – also called white fused alumina (WFA) – does not withstand such a high horizontal load, but its resistance to sample fracture slowly decreases with broader displacement. This evolution is characteristic of materials that exhibit low resistance to crack formation and high resistance to crack propagation. In this case the porosity of the castable is able to absorb the energy of crack propagation until the sample splits completely.

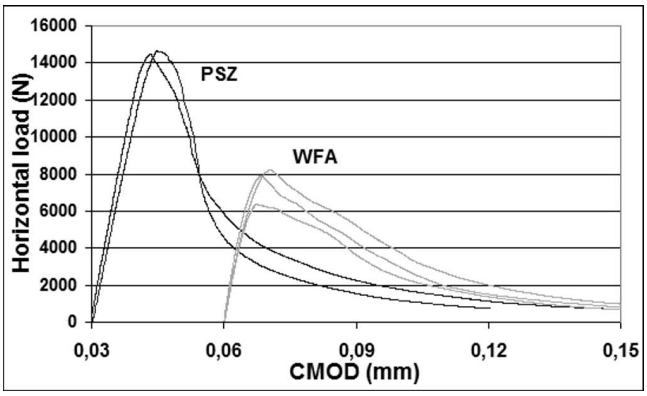

Fig. 1: Horizontal load x CMOD displacement-curves of the two castable formulations studied [Source: B. Schickle *et al.*, 53rd International Colloquium on Refractories, Aachen, Germany, (2010)].

From this wedge splitting test, the work of fracture of the two materials has been estimated at 105.3 J/m^2 for PSZ and at 68.6 J/m^2 for WFA. The work of fracture is an important parameter for the characterization of resistance to thermal shocks. According to Hasselman, thermal shock parameters are grouped according to whether they apply to crack initiation or propagation. Equations 1 and 2 represent the thermal shock parameters applied to crack initiation and crack propagation respectively:

$$R = \frac{\sigma_c(1-\nu)}{\alpha E} \quad [°C] \tag{1}$$

$$R'''' = \frac{E \cdot \gamma_{WOF}}{\sigma_c^2(1-\nu)} \quad [cm] \tag{2}$$

Thermo-mechanical specific values as well as damage tolerance parameters of the studied materials are summarized in Table 1. It should be noted that the same approximate value for the coefficient of dilatation has been used for both materials.

On the one hand, the R parameter gives an estimation of the maximum temperature difference that can be withstood by the material prior to the formation of thermal-shock-generated cracks [12]. Assessment of the R parameter can be applied to situations where fracture is either stable or quasi-stable. As shown in Table 1, the R parameter estimated for PSZ is around 66 % higher than the R parameter for WFA.

On the other hand, the R'''' parameter, which is applied to situations where cracks have already been initiated in the microstructure, represents the minimum crack propagation on initiation of thermal stress fracture and is therefore a suitable indicator of crack propagation resistance [12]. The calculated R'''' parameter values shown in Table 1 reveal a thermo-mechanical behavior that is more than twice as stable for the formulation based on electrofused materials. The considerable scatter of the work of fracture with regard to the WFA explains the broad range of possible R'''' values. However, the tendency reveals a more suitable crack propagation resistance for WFA. A precise prediction of the material behavior with regard to quenching conditions can thus be realized based on the implementation of the fundamental mechanical, elastic and thermal properties of the refractory specimen as Hasselman R-parameters. The relevance of the thermal shock parameters defined by Hasselman [13, 14] with regard to heterogeneous materials such as refractory castables is the focus of several studies, which propose either an extension of the Hasselman theory [15] or the definition of a new parameter taking into account the results of wedge splitting test [16].

The determination of the thermal shock parameters is in agreement with the theory presented from the evolution of the wedge splitting test. WFA castable, with a low value of R and a high value of R'''', is more brittle than PSZ castable with a high value of R and a low value of R'''' at room temperature. Another focus of this study will be to determine if such a behavior with regard to crack initiation and crack propagation can be established with help of damping measurements.

II. Experimental Procedure

(1) Material and thermal shocks

Two high-alumina castables were studied. The first one is composed of tabular alumina (Rio Tinto Alcan)

and partially stabilized zirconia [PSZ] (Industriekeramik Hochrhein GmbH). The second formulation is based on white fused alumina [WFA] (Rio Tinto Alcan). The calcium aluminate cement Secar 71 (Kerneos) as well as the additives, namely the deflocculant (FS 40, BASF) and citric acid used as retarder, complete the two formulations. In both compositions, the maximum grain size of the aggregates was 3 mm. Both formulations obey the same Andreassen packing model with a distribution coefficient of 0.26 for a possible comparison of the thermal shock resistance. Prismatic bars were prepared with the dimensions 160 mm × 40 mm × 40 mm.

After being moulded, cured for 48 h in a humid environment and dried at 110 °C for 24 h, the specimens were fired. The WFA samples were soaked at 1500 °C for 6 h at a heating and cooling rate of 2 K/min. The PSZ samples were soaked at 1300 °C for 6 h at a heating and cooling rate of 1 K/min. A lower firing temperature had to be chosen owing to the damage of coarse grains fired at 1500 °C.

Each sample was subjected to thermal shocks in air in accordance with DIN EN 993 – 11 [17]. Each specimen was subjected to a specific number of progressive thermal shocks from one to ten. The tests were performed at four different temperatures in the case of the PSZ samples: 750 – 850 – 950 and 1050 °C. The WFA specimens were only subjected to thermal shocks at 950 °C. After sintering and thermal shock treatment, the microstructure of each castable was investigated by means of scanning electron microscopy (SEM). Therefore, equipment consisting of a LEO 440i microscope providing magnification from 30 up to 100 000 and an integrated energy-dispersive X-ray analysing system (EDX) was used. The microstructure was examined on polished samples previously embedded in a resin to prevent further microstructural damage during polishing. Inspection of the microstructure is performed based on secondary electrons (SE) that generate the topographical effects and back scattering electrons (BSD) that create the contrast owing to the different atomic masses of the studied elements such as zirconia and alumina.

(2) The Impulse Excitation Technique (IET)

The modulus of elasticity and the damping of each sample were measured after each thermal shock cycle in compliance with ASTM E1876 – 07 with the help of a Resonant Frequency Damping Analyser (RFDA) provided by IMCE (Belgium) [18]. The flexural and torsional modes were used with the purpose of the determining Young's modulus, the shear modulus and subsequently Poisson's ratio as well as the flexural and torsional dampings. In this technique, a specimen subjected to proper mechanical boundary conditions in accordance with the expected mode of vibration is excited by a short and light mechanical impulse. The acoustic response is picked up by a microphone and processed according to the frequency and attenuation rate detection. For bars with a square cross-sections excited at the flexural mode of vibration, Young's modulus (E) is calculated using the following equation:

$$E = 0{,}94642 \cdot \left(\frac{m}{b \cdot R^2}\right) \cdot \left(\frac{l}{h}\right)^3 \cdot T \qquad (3)$$

The parameter R is the Grindo sonic output (μs) and is inversely proportional to the flexural frequency, h is the specimen thickness perpendicular to the vibration direction, l is the specimen length, b is the specimen width and T is a geometrical correction factor that depends on the aspect ratio of the specimen (depending on l and h) and Poisson's ratio. The shear modulus (G) is calculated in a similar manner from the torsional frequency. Poisson's ratio (ν) is calculated based on the relation $\nu = [(E/2G)-1]$ with an interactive algorithm, which also improves the E and G precision. The damping (ξ) is commonly calculated using the logarithmic decrement method:

$$\xi = \frac{\delta}{\omega} \qquad (4)$$

The parameter δ is the angular coefficient of the specimen's acoustic response attenuation on a logarithmic scale, and ω is the angular frequency.

$$\delta = \frac{1}{r} \ln\left(\frac{A_i}{A_{i+r}}\right) \qquad (5)$$

The parameter A_i corresponds to the amplitude of the peak point in the time sinusoidal signal decay function, A_{i+r} is the amplitude of the peak point r cycles later in the time history.

And for a possible comparison of the results, the same experimental geometric conditions were considered. First of all, an automatic positioning sample holder was used to impose the mechanical boundary condition so that the flexural nodes could be predominantly excited. The distance between the microphone and the samples was kept to 5 mm and the distance between the impulse actuator and the sample was kept to 2 mm. The intensity of the impulse excitation was the same for all samples and previously chosen to minimize any non-linearity acoustic response [19]. For possible estimation of Young's modulus, the shear modulus and Poisson's ratio, the sample holder apparatus was used in a flexural/torsion mode.

III. Results and Discussion

(1) Results and discussion of experiments conducted on the PSZ samples

(a) *Elastic properties*

Fig. 2 shows the retained Young's modulus values of the PSZ samples as a function of the number of thermal shock cycles at different tested temperatures (750, 850, 950 and 1050 °C). It is worth mentioning first and foremost that the tested temperature differences for the quenching test are much higher than the maximum temperature calculated in Table 1 that can be withstood by the PSZ specimen prior to the formation of cracks ($\Delta T >> R$). In such experimental conditions, quick formation of a crack network is expected to take place during the first thermal shock, while the further quenching tests enable the characterization of the material with regard to crack propagation resistance. For any thermal shock temperature variation, a two-step decrease of the modulus of elasticity is observed. The two first cycles turn out to be severe enough for crack nucleation to occur within the matrix and cause the depletion of the elastic property. This decrease becomes all the more noticeable

as the temperature change increases. Thus after the whole series of tests, the higher the thermal shock temperature variation was, the lower the retained elastic property became. Thermal shock in air at 1050 °C is so severe that the measurement of the elastic properties reveals more considerable scatters after the last and tenth cycle than those observed up to the ninth thermal shock cycle. Therefore, the questionable results determined on samples close to failure after the 10th thermal shock cycle are not illustrated in Fig. 2. After ten thermal shock cycles, the retained modulus of elasticity is the highest for a thermal shock temperature change (ΔT) of 750 °C with 82.5 % followed by a ΔT of 850 °C, 950 °C and 1050 °C after nine thermal shock cycles for the last mentioned case with respectively 74 %, 57 % and finally 43.5 %. It is worth mentioning that the Young's modulus evolution of 750 °C and 850 °C follows the same tendency while that of 950 °C and 1050 °C stand out from the two first quoted curves. This thermal shock temperature variation of 950 °C is therefore higher than the critical temperature difference defined by Hasselman and leads to crack nucleation, crack propagation and the unification of cracks [20].

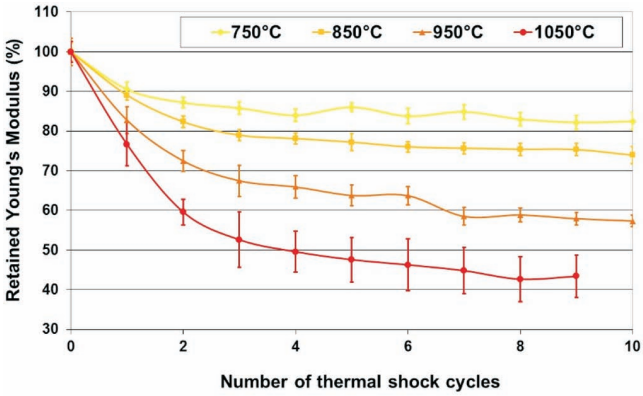

Fig. 2: Evolution of the retained Young's modulus of the PSZ castable with the number of thermal shock cycles at different tested temperatures (750 – 850 – 950 and 1050 °C).

Fig. 3 shows the retained flexural damping values of the PSZ samples as a function of the number of thermal shock cycles at different testing temperatures (750 – 850 – 950 and 1050 °C). As expected, the damping changes follow the inverse tendency of the retained Young's modulus and increase with the formation of cracks and microcracks. The more the cracks propagate within the matrix, the higher the damping. Thus after the whole series of tests, the higher the magnitude of temperature change, the higher the retained flexural damping. After ten thermal shock cycles, the retained flexural damping is lower for a thermal shock temperature variation (ΔT) of 750 °C with 360 % followed by a ΔT of 850 °C, 950 °C and 1050 °C after nine thermal shock cycles for the last mentioned case with respectively 800 %, 1500 % and finally 2500 %. Damping values do not change as a two-step process. Indeed, damping increases proportionally with the damage increase at low thermal shock temperature variations (750 and 850 °C) but turns out to be more difficult to model at higher thermal shock temperature differences (950 and 1050 °C). Experiments conducted at a thermal shock temperature change of 1050 °C combined with the microstructural examination leads to the conclusion of a four-step evolution of the microstructural changes. Up to and including the second cycle, crack nucleation at the level of the grain boundaries causes the first increase of the damping measurements up to 1000 %. The second increase reaching 2000 % of the initial value occurring up to and including the fifth cycle can be explained by the propagation of the cracks within the matrix and throughout the Al_2O_3 aggregates. This step is followed by a steady state up to and including the eighth cycle while the cracks have to consume a lot of energy in order to bypass the ZrO_2 aggregates. Finally, the unification of cracks occurs during the ninth cycle, this network of cracks explains the depletion of the elastic properties and the further difficulties in achieving realistic damping values over 2500 % of the initial value.

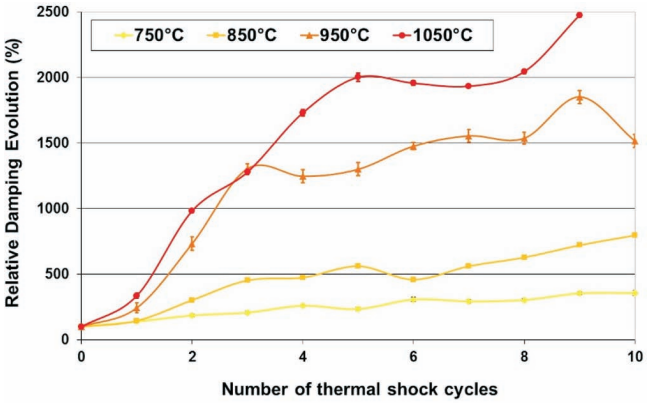

Fig. 3: Evolution of the retained flexural damping of the PSZ castable with the number of thermal shock cycles at different tested temperatures (750 – 850 – 950 and 1050 °C).

Table 1: Thermal shock parameters applied to crack initiation and crack propagation of WFA and PSZ refractory castables at room temperature.

	γ_{WOF} (J/m^2)	ν	α (K^{-1})	E (GPa)	σ_c (MPa)	R (°C)	R'''' (mm)
WFA	68.6 [±8.4]	0.135 [±0.018]	≈ 8.10^{-6}	94.75 [±4.76]	18.25 [±1.43]	20.8 [±3.3]	22.6 [±9.4]
PSZ	105.3 [±7.6]	0.160 [±0.008]	≈ 8.10^{-6}	104.61 [±3.36]	34.38 [±1.19]	34.5 [±2.7]	11.1 [±2.2]

(b) ***Microstructural examination***

The microstructure of the studied castables was examined by means of SEM analyses on polished samples after each thermal shock. Figs. 4 – 7 show the homogeneous distribution of zirconia grains and Al_2O_3 aggregates in the matrix made of hibonite crystals or calcium hexa-aluminate CA_6 particles and monocalcium dialuminate CA_2. The small amount of facets CA_6 in the microstructure because of a low sintering temperature indicates that the PSZ matrix is composed mainly of CA_2 particles. Because of the thermal expansion mismatch between the grog grains and the matrix, cracks nucleate at the level of the grain boundaries after the sintering and the first thermal shock cycle, as can be seen in Fig. 4.

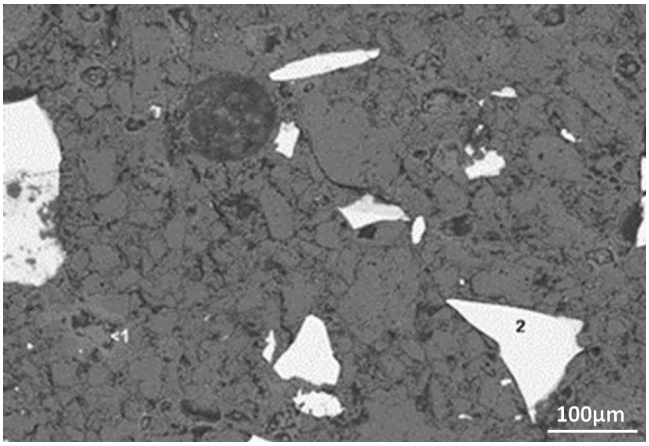

Fig. 4: Crack nucleation at grain boundaries of the PSZ castable after one thermal shock cycle in air at 1050 °C.

The second step of microstructural changes is illustrated in Fig. 5. After propagating along the grain boundaries and within the matrix, which is much more fragile than the aggregates, the cracks are able to propagate throughout the grog grains of alumina. Tabular alumina grains contain a non-negligible inner porosity and inclusions of Na_2O. Because of this physical state, crack propagation within Al_2O_3 grog grains is made easier.

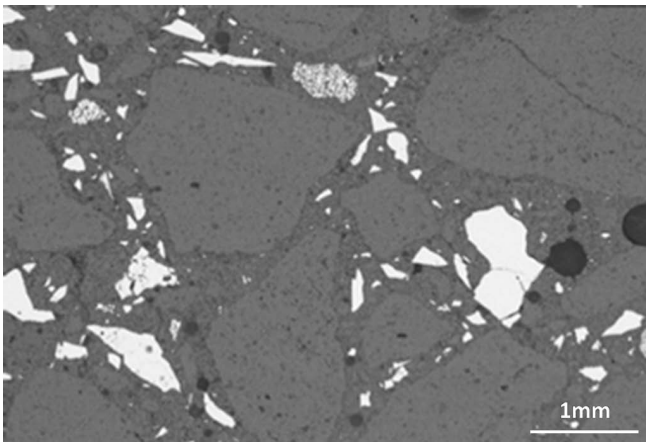

Fig. 5: Crack propagation within the matrix and throughout the Al_2O_3 aggregates of the PSZ castable after three thermal shock cycles in air at 1050 °C.

Then cracks have to bypass the zirconia grains that apply radial stresses in the matrix, as shown in Fig. 6. This crack bridging phenomenon consumes a lot of energy and is responsible for the martensitic transformation of tetragonal grains into monoclinic ones, sometimes causing crack closure. Microcracks are formed from this transformation, which is characterized by volume expansion at the level of the grain boundaries. Those microcracks can later absorb the energy of another crack's propagation. The combination of these mechanisms can explain the steady state of damping changes, testifying to the ability of such a refractory formulation to counter damage to the sample.

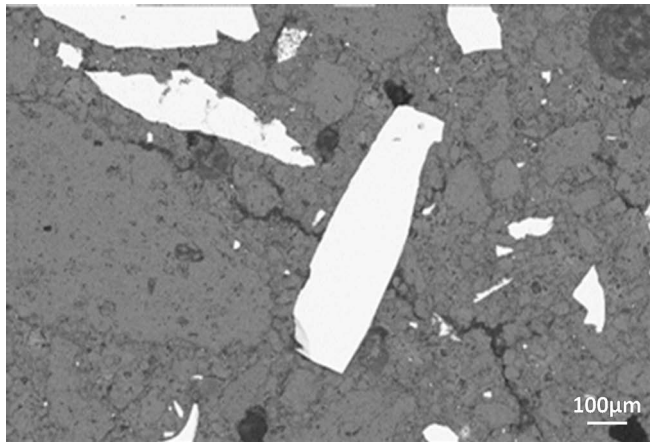

Fig. 6: Crack deviation along zirconia grains of the PSZ castable after five thermal shock cycles in air at 1050 °C.

After nine thermal shocks the crack density within the sample's microstructure is so high that cracks can become unified. In addition to this, the cracks are now able to progress throughout the zirconia grains, as illustrated in Fig. 7. That explains the sudden depletion of the elastic properties and the irreversible damage to the samples. Thus, damping measurements are difficult to monitor.

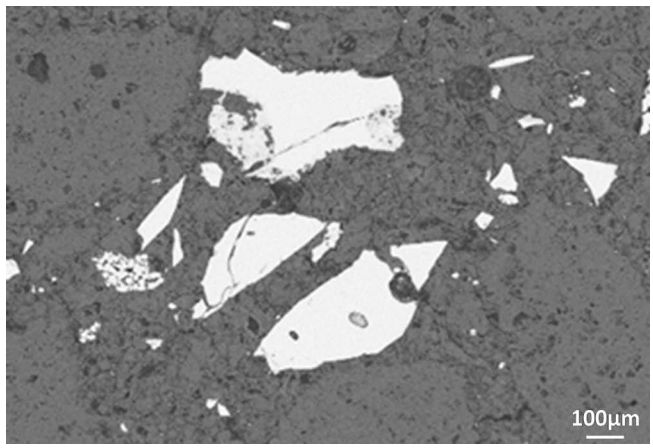

Fig. 7: Unification of cracks and crack propagation throughout ZrO_2 aggregates of the PSZ castable after nine thermal shock cycles in air at 1050 °C.

(2) Results and discussions of experiments conducted on the WFA samples

(a) ***Elastic properties***

Fig. 8 shows the evolution of the retained modulus of elasticity and the retained flexural damping of WFA samples as a function of the number of thermal shock cycles in air at 950 °C. Their Young's modulus follows the same tendency as that of PSZ, in other words a strong decrease

is this property is noticeable up to 70 % after just one thermal shock followed by a steady decrease until the end of the experiment up to 40 %. However, this property depletion is more important for WFA than for PSZ at the same tested temperature: it shows the relevance of the addition of partially stabilized zirconia grains in a standard formulation, and more stable and more thermal-shock-resistant interfaces between matrices and aggregates in the tabular-alumina-based formulation compared to that based on white fused alumina with regard to this kind of thermal shock in air. The theoretical more suitable crack propagation resistance of WFA estimated based on calculation of the Hasselman R'''' parameter is not highlighted with the estimation of the residual stiffness of the material after the quenching test. This shows that the assessment of those thermal shock parameters defined by Hasselman should be discussed, particularly when toughening mechanisms are likely to occur in presence of thermal stress, as can be the case with addition of partially stabilized zirconia particles to a high-alumina castable formulation. It is worth mentioning that a more important decrease in Young's modulus appears after the eighth thermal shock cycle, which correlates with an important increase in the damping values. Damping evolution can nevertheless follow several models of interpretation: damping may proportionally increase with the number of thermal shock cycles. If the uncertainty of the measurement is taken into account, damping values oscillate around a proportional model in that case. A logarithmic evolution is nevertheless conceivable: damping values increase strongly during the first thermal shock cycles and then this increase becomes less notable.

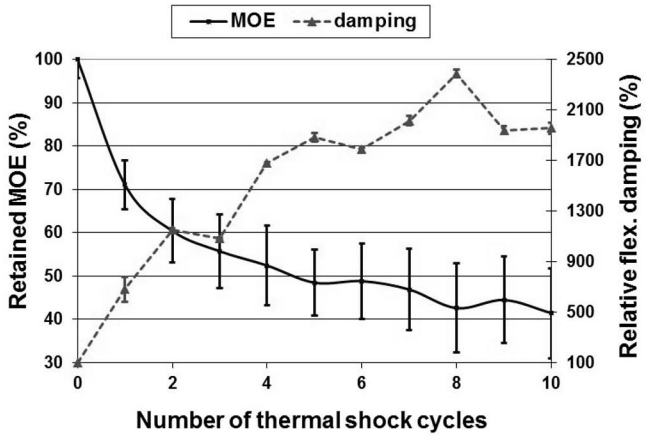

Fig. 8: Evolution of the retained Young's modulus and the retained flexural damping of the WFA castable with the number of thermal shock cycles at 950 °C.

(b) ***Microstructural examination***

The aggregates of white fused alumina as an electro-fused raw material exhibit low inner porosity, as shown in Fig. 9. This raw material with a very low specific surface area is not as reactive as tabular alumina, which corresponds to a sintered raw material. That is the reason why the connection between the dense grains of alumina is really low: the edges of the grains are straight and open gaps between matrix and aggregates are obvious.

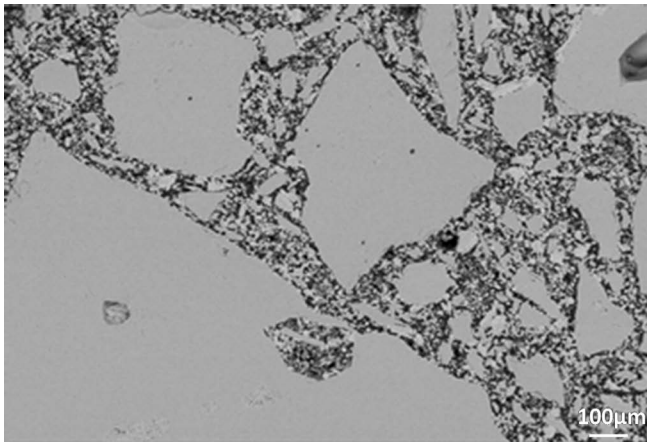

Fig. 9: Microstructural overview of the WFA sample after one thermal shock cycle in air at 950 °C.

After ten thermal shock cycles, the grog grains of white fused alumina present a non-negligible inner porosity. Unlike with the PSZ formulation, the stresses induced by the temperature difference of the thermal shock do not cause any crack nucleation within the matrix because of this obvious low degree of connection between the grains. The damaging of the largest alumina crystals may be mainly responsible for the damping increase as shown in Fig. 10. The formation of a crack network throughout the matrix of WFA samples after thermal shocks is theoretically expected as the stiffness of the material drastically decreases during the whole set of thermal shock cycles and as the tested temperature difference is much higher than the maximum temperature calculated in Table 1 that can be withstood by the WFA sample prior to the formation of cracks ($\Delta T >> R$).

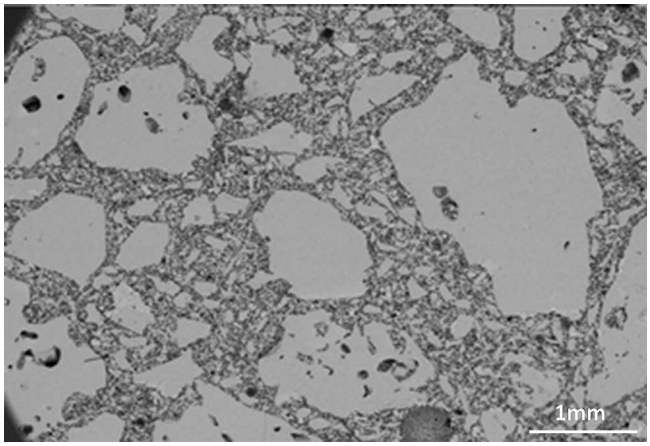

Fig. 10: Damage to the WFA aggregate after ten thermal shock cycles in air at 950 °C.

Moreover, it should be noted that the apparent porosity of WFA castable is much higher than that of PSZ (18.9 % for PSZ compared with 20.0 % for WFA). This difference is essentially due to the low reactivity of electrofused grains, which results in the low degree of connection between the grains, while the packing model before sintering is the same as PSZ. In such a microstructural configuration, where tabular alumina and zirconia grains are more embedded into the matrix by ceramic bonds than the aggregates of white fused alumina, such WFA aggregates exhibit a higher liberty of movement, which entails a higher

damping value after sintering (429.10^{-6} for WFA against 389.10^{-6} for PSZ). From this standpoint, the internal friction mainly depends on the interfaces between the aggregates and the matrix for crack-free materials. The required mechanical excitation for damping measurement can cause local friction phenomena at the interface between white fused alumina and the matrix that cannot generally take place in denser microstructures such as PSZ.

IV. Conclusions

The evolutions of the retained Young's modulus and the flexural damping with the number of thermal shock cycles are strongly correlated. The lower the Young's modulus, the higher the damping. However, the damping evolution provides more information about the microstructural changes. This statement is documented by SEM analyses. Thus in formulations with a high degree of connection between the grains and an optimal packing model, like the PSZ formulation, damping values evolution may be explained based on a defined sequence of microstructural changes:

- crack formation at the level of the grain boundaries,
- crack propagation within the matrix and throughout the Al_2O_3 aggregates,
- crack deviation by partially stabilized zirconia grains,
- unification of cracks and crack propagation throughout ZrO_2 grains.

In formulations with a higher open porosity, like the WFA formulation, interpretation of the damping changes is more challenging. In this case, cracks cannot nucleate and propagate within the matrix because of a low degree of connection between the grains. The induced stresses therefore lead to damaging of the grog grains and the energy provided by those thermo-mechanical stresses is partially absorbed by the open porosity. Besides this, the high porosity and homogeneous distribution of the pores lead to an increase in the internal friction, higher nominal damping values and to dissipation of the energy.

Based on the determination of the thermal shock parameters, materials can be classified according to whether they are resistant to crack initiation or crack propagation. Damping measurements lead to the identification of the microstructural changes in dense refractory materials and reveal the degree of liberty of movement of aggregates in porous materials. The examination of the microstructure therefore emerges as necessary for the interpretation of this elastic characteristic. Nevertheless, damping shows the microstructural damage that could not be detected either by means of SEM or with help of Young's modulus assessment. Damping measurements provide information at a high level of damage while the modulus of elasticity and the resistance to horizontal load do not show any change.

Non-linear effects caused by crack formation and anisotropy of the aggregates are all the more important when the defect density is high. Therefore damping measurements have to be carefully interpreted according to the quantity of thermal stresses induced by the thermal shock procedure.

Acknowledgements

The authors would like to express their sincere thanks to the DFG Project "Evaluation of the damage on refractory materials after thermal shocks with the measurement of the damping and of the resonant frequency" within the framework of SPP 1418 (reference number: TE 146/30 – 1) for financial support.

References

1 Tonnesen, T., Telle, R.: Thermal shock damage in castables: Microstructural changes and evaluation by a damping method, *cfi/Ber. DKG*, **84**, [9], E132 – 6, (2007).

2 Mielczarek, A., Fischer, H., Riehemann, W.: Amplitude-dependent damping of PSZ with sinter defects, *Mat. Sci. Eng. A*, **442**, 488 – 491, (2006).

3 Pereira, H.A., Nascimento, R.C., Rodrigues, J. de A.: Effect of non-linearity on Young's modulus and damping characterisation of high alumina refractory castables through the impulse excitation technique, 53rd International Colloquium on Refractories (2010) Aachen, Germany, Proceedings, 90 – 93

4 Johnson, P.A., Zinszner, B., Rasolofosaon, N.J.: Resonance and elastic nonlinear phenomena in rock, *J. Geophys. Res.*, **101**, [B5], 11553 – 11564, (1996).

5 Abeele, K.V.D., Visscherb, J.: Damage assessment in reinforced concrete using spectral and temporal nonlinear vibration techniques, *Cement Concrete Res.*, **301**, 453 – 1464, (2000).

6 Liang, C., Liu, T., Xiao, J., Zou, D., Yang, Q.: The damping property of recycled aggregate concrete, *Constr. Build. Mater.*, **102**, 834 – 842, (2016)

7 Braulio, M.A.L., Cintra, G.B., Li, Y.W., Pandolfelli, V.C.: Aggregate effects on the thermal shock resistance of spinel-forming refractory castables, *Refractories Worldforum*, **2**, 102 – 106, (2010).

8 Primachenko, V., Martynenko, V., Shulik, I., Kushchenko, P., Paschenko, N.: The influence of sintered or fused MgO-stabilized ZrO_2 on properties of zirconia products, Proc. UNITECR 2007, 268 – 271, (2007)

9 Schnieder, J., Lynen, L., Traon, N., Tonnesen, Th., Telle, R.: Crack formation and shape of fracture surface in tabular-alumina-based castables with addition of specific aggregates, *J. Ceram. Sci. Tech.*, **5**, [2], 131 – 136, (2014).

10 Miyaji, D.Y., Tonnesen, T., Rodrigues, J. de A.: Fracture energy and thermal shock damage resistance of refractory castables containing eutectic aggregates, *Ceram. Int.*, **40**, [9], 15227 – 15239, (2014).

11 Schickle, B., Telle, R., Tonnesen, T., Changes of the mechanical and elastic properties of castables as a function of thermal shock cycles, 53rd International Colloquium on Refractories (2010) Aachen, Germany, Proceedings, 86 – 89, (2010).

12 Lee, W.E., Rainforth, M.: Ceramic microstructures: property control by processing, *Mater. Corros.*, **47**, [6], 346 – 347, (1996).

13 Hasselman, D.P.H.: Unified theory of thermal shock fracture initiation and crack propagation in brittle ceramics, *J. Am. Ceram. Soc.*, **52**, 600 – 604, (1969).

14 Hasselman, D.P.H., Thermal stress resistance parameters for brittle refractory ceramics: A compendium, *Amer. Ceram. Soc. Bull.*, **49**, 1033 – 1037, (1970).

[15] Salvini, V.R., Pandolfelli, V.C., Bradt, R.C.: Extension of Hasselman's thermal shock theory for crack/microstructure interactions in refractories, *Ceram. Int.*, **38**, 5369 – 5375, (2012).

[16] Miyaji, D.Y., Otofuji, C.Z., Rodrigues, J. de A.: The load-displacement curve of steady crack propagation: An interesting source of information for predicting the thermal shock damage of refractories, UNITECR 2013 Proceedings, 811 – 816

[17] DIN EN 993 – 11: Determination of resistance to thermal shock, German version CEN/TS 993/11 (2003).

[18] ASTM 1876 – 07: Standard Test Method for Dynamic Young's Modulus, Shear Modulus, and Poisson's Ratio by Impulse Excitation of Vibration. ASTM International, 15, (2007).

[19] Pereira, H.A., Nascimento R.C., Exposito C.D., Martins T., Rodrigues J. de A., Johnson, P.A.: Elastic Moduli, damping and modulus of rupture changes in a refractory castable due to thermal shock damage, 52nd International Colloquium on Refractories, Aachen, Germany, Proceedings, 20 – 23 (2009).

[20] Hasselman, D.P.H.: Role of fracture toughness in the thermal shock resistance of refractories (in German), *Ber. Dtsch. Keram. Ges.*, **54**, 195 – 201, (1954).